scientific reports

OPEN

Experimental study on the influence of recycled aggregate substitution rate on the mechanical properties of recycled aggregate concrete under sulfate erosion conditions

Yan Fu[1]✉, Quanshen Zhao[1], Qi Sun[1], Song Chen[1], Haili Shi[2], Fan Zhang[3] & Chengyu Bai[3]

To investigate the degradation of recycled aggregate concrete (RAC) under sulfate attack, four groups of RAC cubic specimens (168 in total) were prepared. The influence of recycled coarse aggregate (RA) replacement ratio on the mechanical properties of RAC under sulfate exposure was analyzed. Strength degradation at different exposure durations was assessed, and microstructural changes were examined using scanning electron microscopy (SEM). The results show that: (1) both compressive and splitting tensile strengths decrease with increasing RA replacement ratio, with the reduction in splitting tensile strength being more pronounced; (2) the compressive strength initially increases slightly under sulfate exposure, then gradually declines, with higher RA replacement ratios accelerating the degradation; (3) the decrease in splitting tensile strength is slightly greater than that of compressive strength over time; and (4) this decline in splitting tensile strength becomes more significant as the RA replacement ratio increases. Based on the experimental data, predictive models were established for the degradation of compressive and splitting tensile strengths at various sulfate exposure ages, incorporating the effect of RA replacement. These models effectively characterize the strength deterioration behavior of RAC under prolonged sulfate immersion.

Keywords Recycled concrete, Recycled coarse aggregate replacement rate, Sulfate erosion, SEM, Strength decay modeling

Concrete production consumes substantial amounts of non-renewable resources and emits various harmful gases, contributing to serious environmental concerns[1]. To promote environmentally friendly and sustainable urban development, increasing attention has been given to the reuse of construction waste concrete. One common method involves incorporating recycled coarse aggregate (RA), obtained by crushing concrete from demolished structures, into fresh concrete to produce recycled aggregate concrete (RAC)[1,2]. This practice supports resource recycling and reduces environmental impact. Since RA originates from crushed waste concrete, it inevitably contains residual damage and adherent low-strength mortar. As a result, its fundamental properties—such as porosity, water absorption, and strength—differ significantly from those of natural coarse aggregate (NA), leading to differences in the mechanical performance of RAC compared to conventional natural aggregate concrete NAC[2,3]. Xie et al.[4] reported that RAC exhibits failure modes similar to those of NAC. Wu et al.[5] found that the prismatic compressive strength of RAC decreases with increasing RA replacement ratio, even when slump and other workability parameters remain stable. Bai et al.[6] demonstrated that a weak interfacial zone forms between the old and new mortar in RAC, resulting in reduced splitting tensile strength as the RA content increases. Zhang[7] further observed that fully replacing NA with RA adversely affects the long-term mechanical properties and shrinkage behavior of RAC.

[1]4th Construction Co, Ltd of China Construction 5th Engineering Bureau, Luoyang 471023, China. [2]China United Northwest Institute for Engineering Design & Research Co., Ltd., Xi'an 710077, China. [3]Department of School of Civil Engineering, Xi'an University of Architecture and Technology, Xi'an 710055, China. ✉email: FY13572845516@163.com

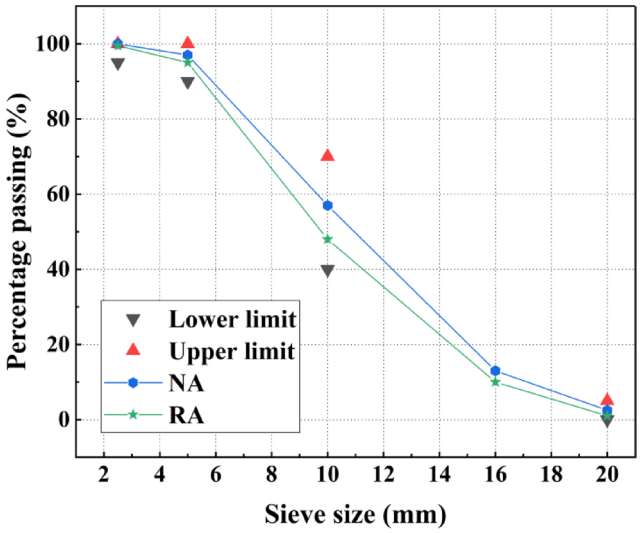

Fig. 1. Particle gradation of coarse aggregate.

Item	Bulk density (kg/m^3)	Apparent density (kg/m^3)	Porosity (%)	Water absorption (%)	Soil content (%)	Water content (%)
NA	1450	2690	46.1	0.72	0.85	0.33
RA	1293	2496	48.2	6.04	0.70	0.59
S	1635	2590	36.9	1.96	0.97	0.63

Table 1. Physical properties of aggregate.

Concrete is frequently exposed to harsh environmental conditions—such as chloride salts, sulfates, wet-dry cycles, and freeze-thaw cycles—throughout its service life, which can lead to cracking, strength loss, and overall performance degradation[8–10]. Among these factors, sulfate attack has been widely recognized as a major cause of deterioration in the mechanical properties of concrete[11–13]. Accordingly, both domestic and international researchers have investigated the degradation mechanisms of concrete subjected to sulfate erosion. These studies generally indicate that the strength of concrete under sulfate exposure follows a typical pattern of initial increase followed by a subsequent decline, regardless of sulfate concentration[13–16]. A lower water–cement ratio improves sulfate resistance and extends the initial strength gain phase, while a higher water–cement ratio shortens this phase[17–19]. However, due to the inferior properties of RA—such as lower strength and higher porosity—compared to NAC, the durability of RAC under sulfate attack differs significantly from that of NAC[20,21]. Only limited research has addressed the sulfate resistance of RAC. Devi et al.[22] reported that the interfacial transition zone between new and old mortar in RAC deteriorates more rapidly under sulfate exposure. Furthermore, as the RA replacement ratio increases, the strength gain during the early stage of sulfate exposure diminishes, and strength degradation accelerates in the later stages[2].

In summary, current research on the sulfate resistance of recycled concrete remains insufficient. To address this gap, the present study experimentally investigates the effects of RA replacement ratio on the mechanical properties of RAC at various sulfate immersion durations. In addition, a predictive degradation model for compressive and splitting tensile strengths is developed, incorporating the influence of RA content and sulfate exposure age. This study provides valuable insights for promoting RAC applications and designing structures in harsh environments.

Materials and methods

Test materials

The cement used in the experiment was P.O. 42.5 ordinary Portland cement, while the recycled coarse aggregate was obtained by crushing and sieving concrete beams demolished in the laboratory, with a tested strength grade of C35. The particle size of the recycled coarse aggregate was controlled within the range of 5–20 mm through screening. The particle size distribution curves of RA and NA, obtained through sieve analysis, are presented in Fig. 1, demonstrating well-graded characteristics of the coarse aggregates. The river sand used had a particle size range of 0.5–3.5 mm, with a fineness modulus of 2.56. The basic physical properties of the NA and RA measured according to the Chinese standard JGJ 52-2006 [23] are shown in Table 1.

Specimen preparation process

Tests were conducted to prepare one type of NAC and three types of RAC with RA substitution rates of 25%, 50%, and 100%, respectively, with NAC serving as the control group. Since the water absorption of RA is significantly

Specimen number	RA MRS (%)	Dosage(kg/m³)							
		C	NA	RA	S	W	AW	WR	WCR
NAC	0	300	1130	0	800	144	0	3.0	0.48
RAC-25%	25	300	847.5	282.5	800	144	14.25	3.0	0.48
RAC-50%	50	300	560	560	800	144	28.5	3.0	0.48
RAC-100%	100	300	0	1130	800	144	57	3.0	0.48

Table 2. Mixture ratio of RAC.

Fig. 2. Sulfate immersion of specimens.

higher than that of NAC additional adsorbed water must be added in advance to maintain a constant water-cement ratio for concrete at each strength level. The amount of additional adsorbed water is calculated as follows.

$$\Delta W = m_{RA}[(S_{RA} - W_{RA}) - (S_{OA} - W_{OA})] \quad (1)$$

Where: m_{RA} is RA mass, W_{RA} is RA natural Water content, W_{OA} is NA natural water content, S_{RA} is RA water absorption, S_{OA} is NA water absorption.

C represents Cement; S denotes River Sand; W refers to Water; AW indicates Additional Water; WR stands for Water Reducer; and WCR is the Water-to-Cement Ratio.

One type of NAC was mixed with three types of RAC, as shown in Table 2. When mixing the RAC, RA and additional water were first added to the mixer and mixed for 2 min, during which time the additional water was largely absorbed by the RA, ensuring that the water-cement ratio remained constant for each admixture. Following this, crushed stone, river sand, cementitious materials, and water were added sequentially and mixed for another 2 min. After testing the fluidity in accordance with the relevant standards, the concrete was molded. The specimens were demolded 24 h after casting and then cured in a standard curing chamber at a temperature of 20 ± 2 °C and a relative humidity exceeding 95% for 28 days.

Test program

Forty-two specimens were prepared for each mix ratio. After standard curing, six specimens from each group were removed for natural drying and subsequently tested for compressive strength and splitting tensile strength to evaluate the baseline mechanical properties prior to sulfate exposure. The remaining specimens were divided into six batches and immersed in a 5% Na_2SO_4 solution for sulfate erosion testing at different exposure durations: 60, 120, 180, 240, 300, and 360 days, as shown in Fig. 2. To ensure full and uniform contact between the RAC specimens and the sulfate solution, each specimen was spaced 30 mm apart, with 20-mm-thick wooden strips placed between layers to maintain vertical separation. The liquid level was maintained at least 30 mm above the top surface of the uppermost specimen throughout the immersion period. The sulfate solution was replaced every 30 days to maintain stable concentration and pH. At each designated exposure age (60, 120, 180, 240, 300, and 360 days), one batch of specimens was removed from the solution, allowed to dry naturally, and then tested for cubic compressive strength and splitting tensile strength, as illustrated in Fig. 3.

Analysis of test results

Experimental phenomena

No significant external damage was observed on the specimens after sulfate erosion; however, a layer of white sulfate crystals precipitated on the surface. This crystalline layer thickened with increasing immersion time. During the compressive strength tests, specimens with shorter sulfate exposure durations and lower RA replacement ratios exhibited fewer surface cracks under loading and displayed more brittle behavior. As RAC specimens experienced prolonged sulfate erosion, their compressive strength decreased, the number of vertical

(a) (b)

Fig. 3. Test loading diagram. (**a**) Cube compressive test (**b**) Split tensile test.

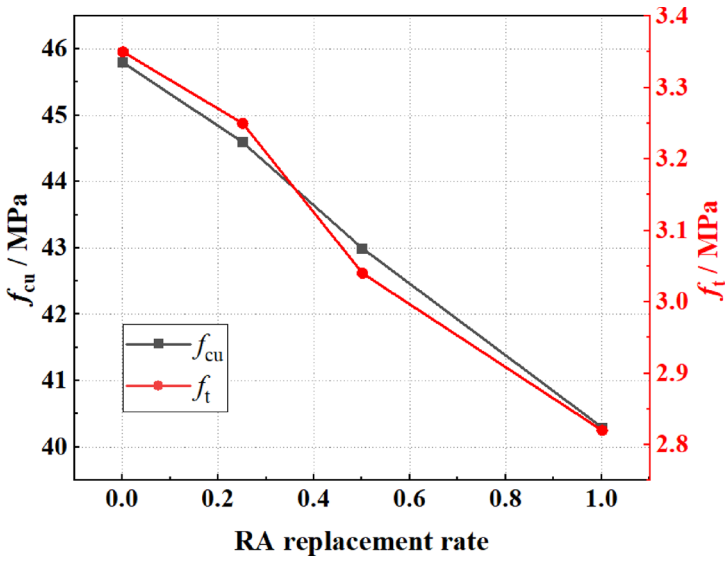

Fig. 4. Effect of RA replacement rate on RAC strength.

cracks on the surface increased during loading, and deformation at failure became more pronounced. The brittleness of the specimens diminished, with this effect becoming more evident at higher RA replacement ratios.

Observations from the splitting tensile tests showed that, for NAC, splitting damage primarily occurred at the interface between mortar and aggregate, with minimal damage to the aggregate itself. With the incorporation of RA, the damage surfaces gradually exhibited detachment of RA particles, while damage at the mortar–aggregate interface decreased. Consequently, the splitting tensile strength of the specimens declined, accompanied by a reduction in brittleness. This behavior is mainly attributed to the lower strength and higher brittleness of RA. Some studies[10–12] have indicated that the bond between fresh cement paste and RA is stronger; however, microstructural analyses and damage mechanism studies confirm that the overall brittleness of RAC is reduced.

Examination of the splitting surfaces of RAC specimens at different erosion ages revealed no significant differences in the morphology of splitting damage, except for a reduction in brittleness as the erosion age increased. This reduction is attributed to the accumulation of volume-expanding products, such as cement hydration products and sulfate reaction products, within the RAC over time. These expansive products induce internal microcracks due to volumetric expansion. During splitting tensile tests, internal cracks propagated along these microcracks, resulting in decreased resistance to splitting failure.

RA effect on RAC strength

Figure 4 illustrates the variation curves of compressive strength (f_{cu}) and splitting tensile strength (f_t) of RAC with increasing RA substitution rates under uneroded conditions. It is evident from the figure that both compressive

and splitting tensile strengths decrease as the RA substitution rate increases. Compared to NAC, when the RA substitution rate reaches 100%, the compressive strength of the specimen decreases by 5.5 MPa, and the splitting tensile strength decreases by 0.53 MPa. This indicates that incorporating RA adversely affects the strength of RAC. This is primarily because a small amount of adhered cement mortar on RA is significantly weaker than the original coarse aggregates. Additionally, RA causes secondary damage to the primary coarse aggregates during the crushing process, which may lead to further deterioration of the concrete. The secondary damage incurred during crushing results in more initial microcracks in the RA used to prepare RAC, thereby causing a reduction in RAC strength as the RA substitution rate increases, even when the water–cement ratio remains constant.

As shown in the RAC strength variation curve in Fig. 5, the rate of decrease in splitting tensile strength is greater than that of compressive strength, and this difference becomes more pronounced with increasing RA substitution rate. When the RA substitution rate is low (25%), the difference in decline rates between compressive and splitting tensile strengths is only 0.36%. However, as the RA substitution rate increases to 50%, the difference rises significantly to 3.14%. This difference further increases to 3.8% when RA is used exclusively as the coarse aggregate. This phenomenon can be primarily attributed to the initial cracks generated during the crushing of RA. As the proportion of RA increases, the accumulation of these initial cracks also increases, resulting in a greater number of internal cracks in RAC with higher RA substitution rates. Additionally, a significant amount of mortar adheres to the surface of the crushed RA, but it is not tightly bonded to the internal crushed stone. The complexity of the bond between the fresh mortar and RA in the formation of fresh concrete causes the transition zone at the RA–new mortar interface to become a weak zone, thereby reducing RAC's resistance to splitting. This leads to the observed greater decrease in splitting tensile strength.

Deterioration pattern of RAC strength with erosion age

Compressive strength evolution under sulfate erosion

Figure 6 shows the changes in compressive strength of the specimens after sulfate erosion. Analysis of the curve reveals that the compressive strength of RAC can be divided into two stages: an initial rising phase during the early erosion period and a subsequent declining phase during the later erosion period. The strength gain of RAC with different RA substitution rates varies in the early stage, as does the rate of strength decline in the later stage. When the RA substitution rate is below 50%, the peak compressive strength occurs around 120 days of erosion age. As the RA substitution rate increases, the peak compressive strength occurs earlier, reaching its maximum at 60 days when the RA substitution rate is 100%, followed by a decline.

As shown in Fig. 7, which illustrates the rate of change in RAC compressive strength after sulfate erosion, the increase in compressive strength during the early phase decreases as the RA substitution rate increases. The peak compressive strength increases by 6.3%, 5.2%, 5.1%, and 3.0% at RA substitution rates of 0%, 25%, 50%, and 100%, respectively, compared to the uneroded specimens. In the later stages of erosion, the rate of compressive strength reduction accelerates with increasing RA substitution rate. By the time the immersion age reaches 360 days, the compressive strength decreases by 11.6%, 14.5%, 15.6%, and 20.1% for specimens with RA substitution rates of 0%, 25%, 50%, and 100%, respectively, compared to the uneroded specimens.

This phenomenon is mainly attributed to the reaction of sulfate ions (SO_4^{2-}) in the sodium sulfate solution with calcium hydroxide ($Ca(OH)_2$), a cement hydration product, and C–S–H gel during the early stages of immersion, forming volume-expanding products such as ettringite (AFt) and gypsum ($CaSO_4{\cdot}2H_2O$). These products fill small voids within the RAC, densifying the material. Additionally, RAC is not fully hydrated at the end of the curing period; therefore, the specimens are more compact and continue hydrating when immersed

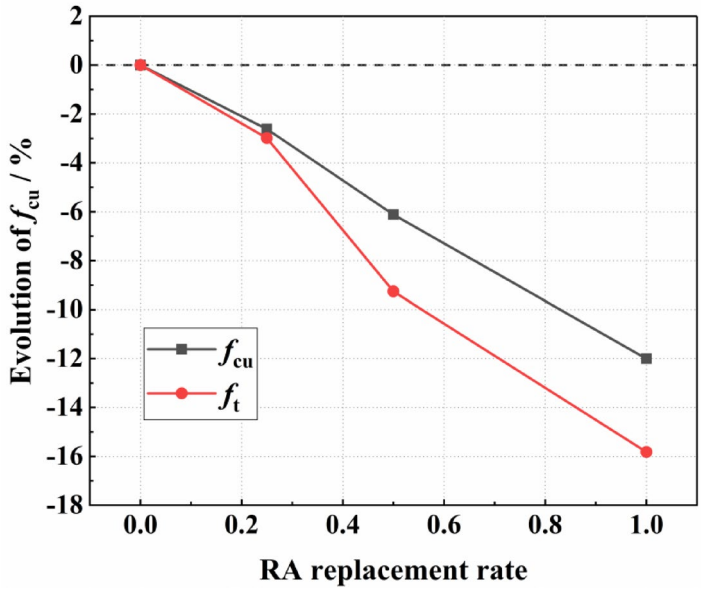

Fig. 5. RAC intensity rate of change curve.

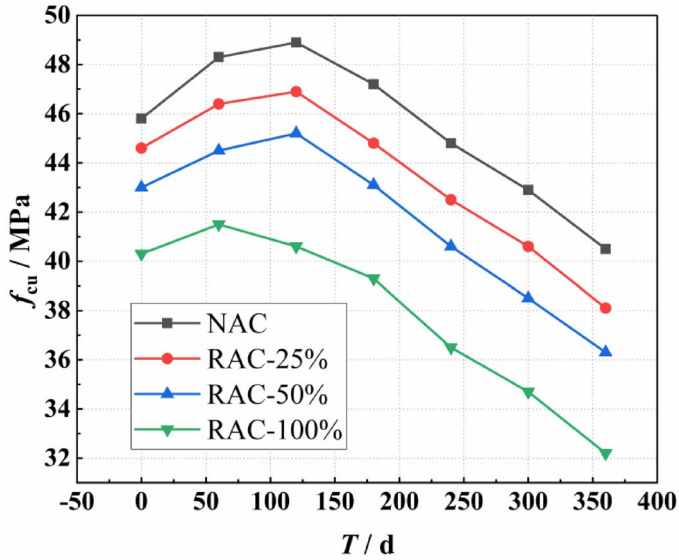

Fig. 6. The variation trend of RAC compressive strength with erosion time.

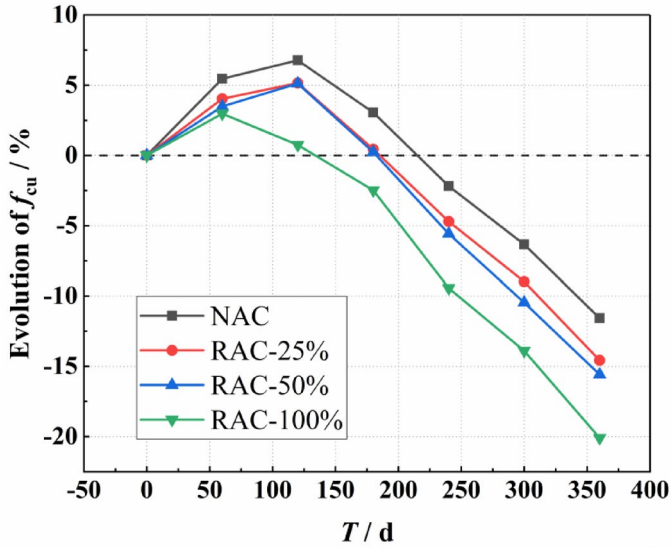

Fig. 7. Rate of change curve of RAC compressive strength after erosion by sulfate erosion.

in the sulfate solution, resulting in a slight strength increase. Furthermore, RA possesses high porosity and strong water absorption characteristics. As the RA substitution rate increases, the porosity of RAC increases, accelerating cement hydration during the curing period for higher RA substitution rates. This leads to a higher degree of hydration at the end of curing in RAC with higher RA content, which in turn reduces strength growth during the early stages of sulfate immersion.

As the immersion time increases, volume-expanding products such as ettringite and gypsum continue to accumulate inside the RAC, generating internal microcracks. These cracks develop further with prolonged immersion, causing initial damage to the specimens. Moreover, the higher the RA substitution rate, the more vulnerable the RAC is to sulfate ion penetration, accelerating the rate of strength deterioration.

Splitting tensile strength evolution of RAC under sulfate erosion

Figure 8 shows the trend of RAC splitting tensile strength with increasing erosion time. It can be observed that the variation in splitting tensile strength under different sulfate erosion ages follows a pattern similar to that of compressive strength. However, compared to compressive strength, the increase in splitting tensile strength during the pre-erosion period is smaller, while the decrease during the post-erosion period is more pronounced. As shown in Fig. 9, compared to the uneroded specimens, the peak splitting tensile strength of RAC with RA substitution rates of 0%, 25%, 50%, and 100% increased by 2.1%, 1.2%, 2.96%, and 1.8%, respectively. When the

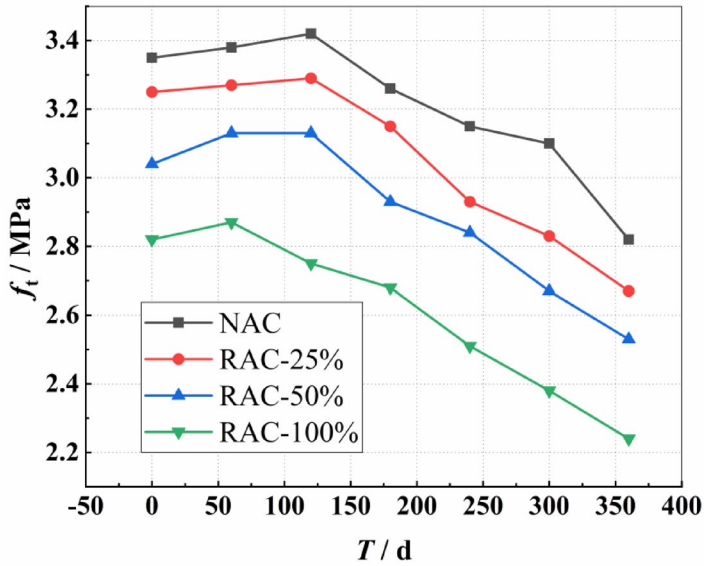

Fig. 8. The variation trend of RAC splitting tensile strength with erosion time.

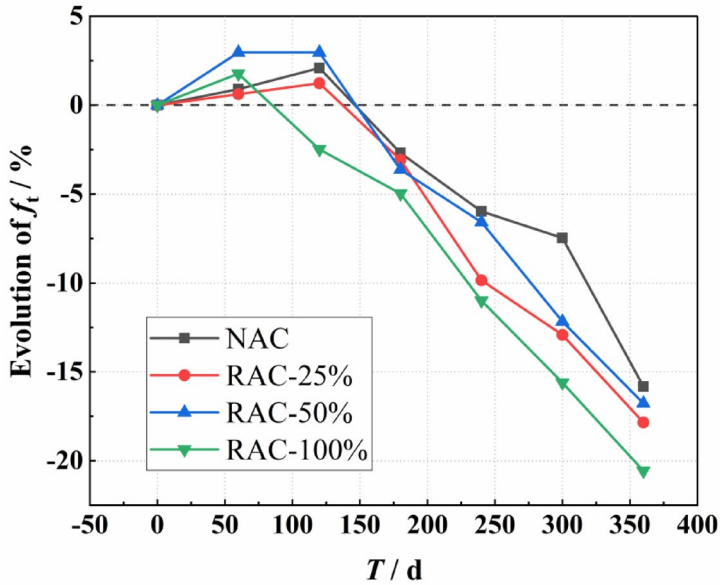

Fig. 9. Rate of change curve of RAC split tensile strength after sulfate erosion.

erosion age reached 360 days, the splitting tensile strengths of RAC with RA substitution rates of 0%, 25%, 50%, and 100% decreased by 12.5%, 12.8%, 17.8%, and 16.8%, respectively. The significant reduction in RAC splitting tensile strength with increasing RA substitution rate under sulfate attack is mainly attributed to the formation of numerous internal cracks caused by volume-expanding products generated through sulfate reactions with cement hydration products. Additionally, initial cracks generated during the crushing of RA accumulate as the RA substitution rate increases, resulting in a higher number of internal cracks in RAC with larger substitution rates. The extensive internal cracking has a more detrimental effect on splitting tensile strength than on compressive strength, leading to the more pronounced decrease observed in RAC splitting tensile strength.

Microstructural analysis of RAC under sulfate erosion

The SEM images of the interfacial transition zone (ITZ) of RAC at different erosion ages are shown in Fig. 10. It is evident from the figure that, when RAC was not subjected to sulfate erosion, a distinct ITZ existed between the RA aggregate and the new mortar. The new cement paste at the interface did not fully fill the voids on the RA surface, leaving some microcracks. As sulfate ions (SO_4^{2-}) infiltrate the RAC through these microcracks and voids, they react with components such as the aluminate phase (e.g., C_3A) and hydration products (e.g.,

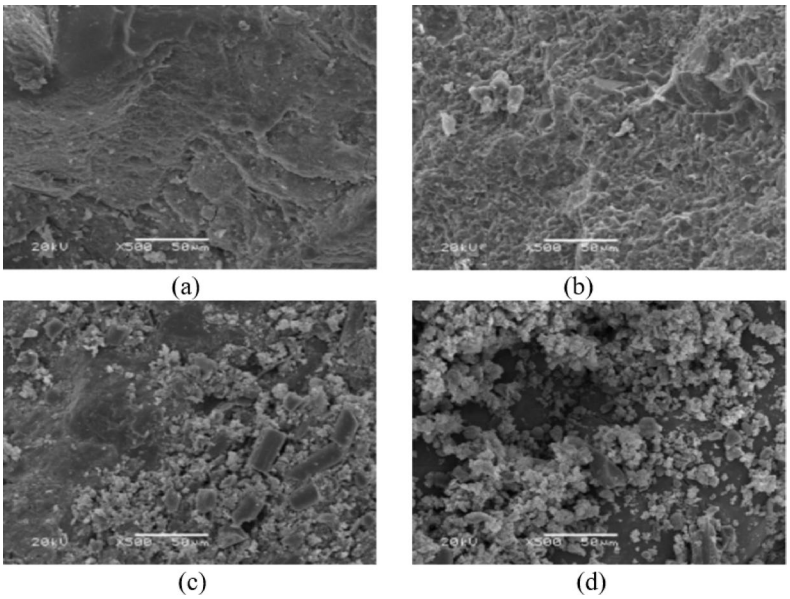

Fig. 10. SEM image of RAC interior after sulfate erosion (RA-50%). (**a**) 0 d, (**b**) 120 d, (**c**) 240 d, (**d**) 360 d.

monosulfate-type calcium sulfoaluminate AFm) in the cement, forming calcium aluminate sulfate hydrate crystals ($3CaO{\cdot}Al_2O_3{\cdot}3CaSO_4{\cdot}32H_2O$).

In Fig. 10b, the distribution of C–S–H gel in the cement paste during the pre-erosion stage appears more uniform. Some unhydrated cement particles undergo further hydration, generating additional C–S–H gel, which enhances the compactness of the paste. A small amount of calcium aluminate sulfate crystals begins to form inside the RAC, filling the voids and microcracks, thereby densifying the microstructure and improving the short-term compressive strength of the concrete.

As the erosion time progresses, calcium aluminate crystals gradually develop into coarse, plate-like structures. Excess sulfate ions react with calcium hydroxide ($Ca(OH)_2$) to form gypsum, as shown in Figs. 9d and 10c. Simultaneously, ongoing formation of calcium aluminate involves water absorption and volumetric expansion. The generation of these expansive products, combined with microcrack propagation, results in increased porosity and reduced compactness of the concrete matrix. When the expansion-induced stress exceeds the tensile strength of the material, internal microcracks further propagate. This explains the significant degradation in compressive and splitting tensile strengths of RAC under long-term sulfate attack. Moreover, the porous old mortar adhered to the surface of recycled aggregate serves as a preferential pathway for sulfate ion penetration, accelerating deterioration of the interfacial transition zone (ITZ). The degradation of the ITZ weakens the bond between aggregate and cement paste, leading to a reduction in the overall mechanical strength of the recycled aggregate concrete.

Figure 11 presents SEM images of the internal microstructure of recycled aggregate concrete (RAC) specimens with varying recycled aggregate (RA) substitution rates after sulfate erosion. The images reveal a marked increase in the accumulation of erosion products, such as calcium sulfate and gypsum, within the specimens as the RA substitution rate rises, particularly at an erosion age of 360 days. Compared to natural aggregate concrete (NAC), RAC exhibits a significantly lower density in the interfacial transition zone (ITZ) with increasing RA content, which can be attributed to the inherently higher porosity of RA and the presence of a greater number of initial microcracks. Under sulfate exposure, sulfate ions more readily penetrate RAC and chemically react with the cementitious matrix. Additionally, as the RA substitution rate increases, the exposed area of the old mortar expands, intensifying sulfate-induced reactions and accelerating degradation of the ITZ. This degradation weakens the bond between aggregate and paste, leading to an accelerated reduction in mechanical strength in RAC with higher RA substitution rates as the erosion period progresses.

Predictive modeling of RAC intensity in sulfate erosion environments

Prediction of compressive strength decay in RAC

After sulfate erosion, the mechanical properties of the concrete deteriorated. To further investigate the degradation of compressive strength under sulfate erosion conditions, a sulfate erosion influence coefficient, β, was introduced as a function of erosion age, T. By analyzing the variation curve of the compressive strength decay rate of specimens in the NAC group, it was observed that the coefficient β follows a cubic function with respect to erosion age T, as illustrated in Fig. 12. Nonlinear fitting of the data in Fig. 11 yields the following expression for calculating β:

$$\beta = -1.18 \times 10^{-8}T^3 + 9.14 \times 10^{-6}T^2 - 0.0015T \tag{2}$$

Combining Eq. (2) gives the formula for calculating NAC compressive strength for different sulfate erosion ages:

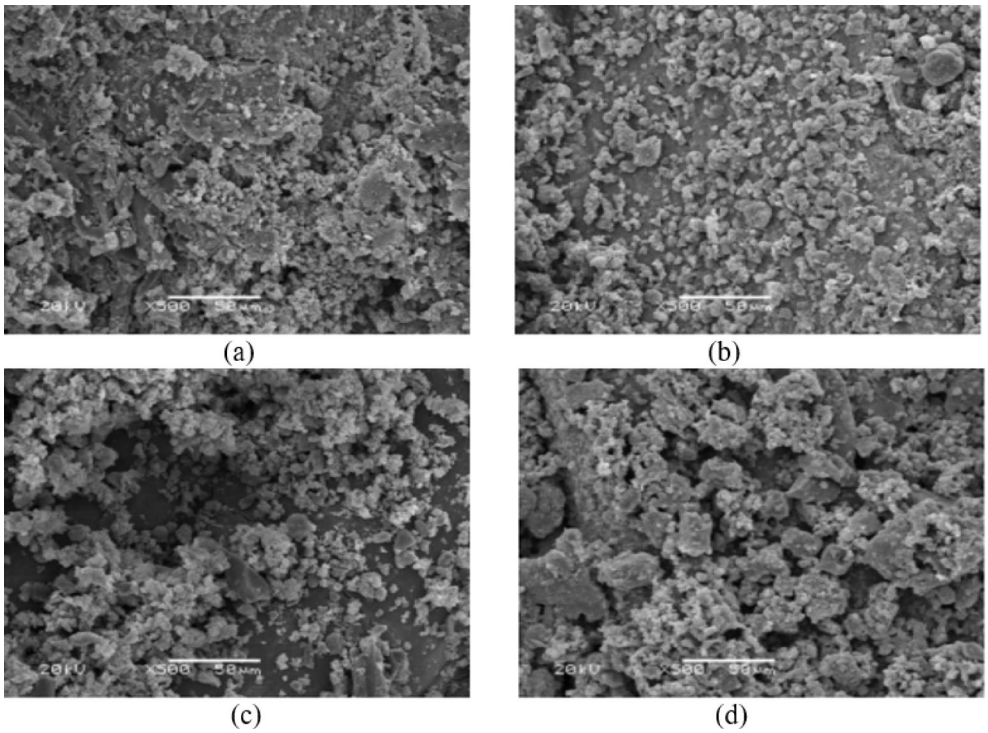

Fig. 11. SEM maps within the RAC for different RA replacement rates (erosion age 360d). (**a**) NAC, (**b**) RAC-25%, (**c**) RAC-50%, (**d**) RAC-100%.

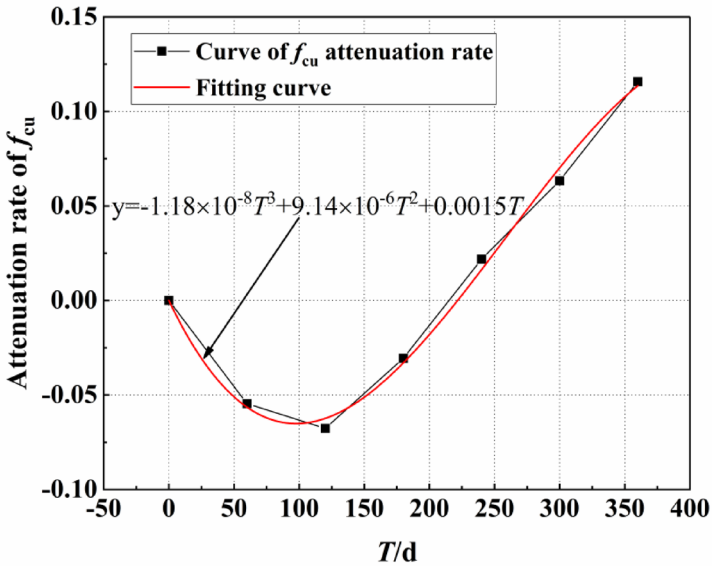

Fig. 12. The attenuation rate curve of compressive strength at different erosion ages.

$$f_{cu,0} = f_{cu,0}(1-\beta) \tag{3}$$

Where: $f_{cu,0}$ is the uneroded NAC compressive strength.

Figure 13 illustrates the compressive strength decay rate curves at different RA substitution rates. The compressive strength decay rate is derived from the ratio of the difference between the calculated values from Eq. (3) and the compressive strength test values for RAC with three different RA substitution rates. As shown in Fig. 13, with the increase in erosion age, the compressive strength decay rate of specimens with all three RA substitution rates generally increases linearly. Moreover, with the increase of RA substitution rate, the compressive strength decay rate of specimens at the same erosion age is approximately directly proportional to

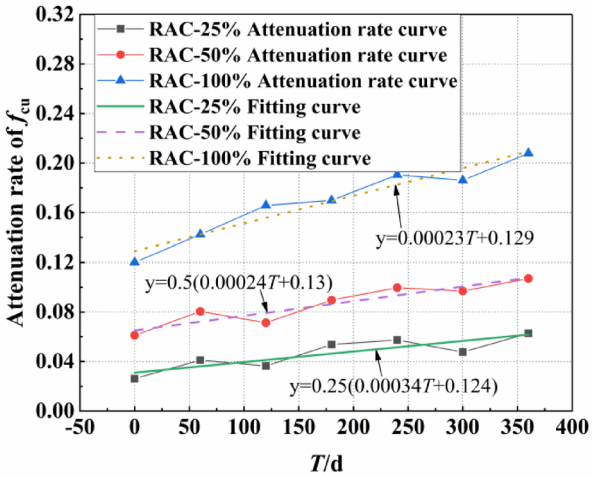

Fig. 13. Attenuation curves of compressive strength of specimens with different RA replacement ratios.

the RA substitution rate, *r*. To reflect the influence of the RA substitution rate on the compressive strength of RAC under sulfate erosion, an RA substitution rate influence coefficient, *γ*, as a function of RA substitution rate r and erosion age *T*, is introduced. By linearly fitting the compressive strength decay rates of the three groups of specimens with different RA substitution rates, and taking the average value of the fitting coefficients from all three groups, the expression for the coefficient of influence *γ* on the compressive strength in relation to the RA substitution rate is derived as follows:

$$\gamma = 1 - r(2.67 \times 10^{-4}T + 0.128) \tag{4}$$

Combining Eqs. (3) and (4) yields the following equation for calculating the compressive strength of RAC, which incorporates the effect of varying RA substitution rates under sulfate erosion conditions:

$$f_{cur,T} = f_{cu,0}(1 - \beta)\gamma \tag{5}$$

Prediction of splitting tensile strength decay in RAC

From the above study, it can be observed that the decay rate of RAC splitting tensile strength is slightly greater than that of compressive strength as the RA substitution rate and erosion age increase. Applying the conventional conversion relationship between compressive strength and splitting tensile strength from existing standards to calculate RAC splitting tensile strength after sulfate erosion tends to overestimate the results compared to experimental values. Therefore, to achieve more accurate predictions of RAC splitting tensile strength post-sulfate attack, it is necessary to introduce an attenuation coefficient for splitting tensile strength that depends on both the RA substitution rate r and erosion age T, and subsequently modify the conversion equation accordingly. By fitting the discrepancies between the standard values and test results, the formula for calculating the splitting tensile strength attenuation coefficient is derived as follows:

$$\phi = 1.2 \times 10^{-5}Tr - 0.00016T - 0.072r + 1 \tag{6}$$

By combining Eqs. (5) and (6), the adjusted conversion equation for RAC splitting tensile strength after sulfate attack is obtained as follows:

$$f_{tr,T} = 0.19\phi\, f_{cur,T}^{0.75} \tag{7}$$

Comparison of experimental and predicted values

By substituting the RA r and T into Eqs. (5) and (7), the predicted curves for RAC compressive and splitting tensile strengths under sulfate erosion are generated, as shown in Fig. 14. The test results cluster closely around these curves, indicating good agreement between the model and experimental data. This confirms that the proposed model effectively captures the influence of RA substitution on RAC strength deterioration under sulfate attack.

Conclusion

This study investigated the effects of RA replacement ratio on the strength performance of RAC under sulfate immersion at various exposure ages. A strength degradation model for RAC in sulfate environments was also developed. The main conclusions are as follows:

(1) With increasing RA replacement ratio, both the compressive strength and splitting tensile strength of RAC show a decreasing trend. The rate of reduction in splitting tensile strength is greater than that of compres-

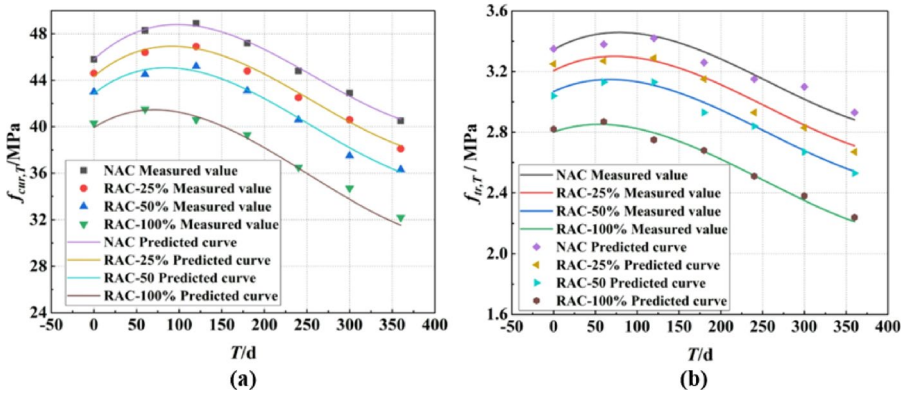

Fig. 14. Comparison of experimental value and predicted value. (**a**) Compressive strength (**b**) Splitting tensile strength.

sive strength. For specimens with 100% RA replacement, the difference in reduction rates between splitting tensile and compressive strengths reaches 3.8%.

(2) At the early stage of sulfate immersion, the strength of RAC initially increases. However, the greater the RA replacement ratio, the smaller the strength gain and the earlier the peak strength occurs. As the exposure duration increases, both compressive and splitting tensile strengths decline. RAC with higher RA content exhibits faster strength degradation, with the decrease in splitting tensile strength slightly exceeding that of compressive strength. After 360 days of sulfate exposure, specimens with full RA replacement show compressive and splitting tensile strength losses of 20.1% and 21.6%, respectively.

(3) As the sulfate exposure period increases, the accumulation of expansive chemical products such as ettringite and gypsum becomes more pronounced. These products promote the propagation of microcracks and increase porosity, resulting in reduced concrete density and deteriorated strength.

(4) A degradation model for compressive and splitting tensile strengths of RAC under sulfate immersion, incorporating the effect of RA replacement ratio, was established. The proposed model effectively captures the deterioration trends of RAC mechanical properties under prolonged sulfate attack.

This study provides a comprehensive investigation into the strength degradation of RAC under sulfate attack. Future research could further explore the effects of different types of recycled aggregates, as well as the strength deterioration of RAC under coupled deterioration mechanisms, such as sulfate erosion combined with freeze-thaw cycles.

Data availability

The data that support the findings of this study are available on request from the corresponding author, [Yan Fu] upon reasonable request.

Received: 27 March 2025; Accepted: 30 July 2025
Published online: 11 August 2025

References

1. Zhang, H. et al. A new look at the resistance of recycled aggregate concrete (RAC) to the external sulfate attacks: the influence of the multiple mesoscopic material phases. *J. Building Eng.* **64**, 105653 (2023).
2. Zhang, H., Ji, T. & Liu, H. Performance evolution of recycled aggregate concrete (RAC) exposed to external sulfate attacks under full-soaking and dry-wet cycling conditions. *Constr. Build. Mater.* **248**, 118675 (2020).
3. Xu, F. et al. The mechanical properties of tailing recycled aggregate concrete and its resistance to the coupled deterioration of sulfate attack and wetting–drying cycles. *Struct. Elsevier.* **27**, 2208–2216 (2020).
4. Xie, F. et al. Experimental investigations on the durability and degradation mechanism of cast-in-situ recycled aggregate concrete under chemical sulfate attack. *Constr. Build. Mater.* **297**, 123771 (2021).
5. Wu, Q., Ma, Q. & Huang, X. Mechanical properties and damage evolution of concrete materials considering sulfate attack[J]. *Materials* **14** (9), 2343 (2021).
6. Bai, W. et al. Study on multi-scale dynamic mechanical properties of Metakaolin modified recycled aggregate concrete under coupling conditions of sulfate attack and dry-wet cycles. *J. Building Eng.* **94**, 109921 (2024).
7. Zhang, H., Xiao, J. & Tang, Y. Long-term shrinkage and mechanical properties of fully recycled aggregate concrete: testing and modelling,cement and concrete composites, **130**, 104527 (2022).
8. Hanbin Cheng, T., Liu, D. & Zou Compressive strength assessment of sulfate-attacked concrete by using sulfate ions distributions. *Constr. Build. Mater.* **293**, 123550 (2021).
9. Wang, K., Guo, J. & Yang, L. Multiphysical damage characteristics of concrete exposed to external sulfate attack: elucidating effect of drying–wetting cycles. *Constr. Build. Mater.* **329**, 127143 (2022).
10. Liu, K. et al. Damage mechanism and mechanical behavior of recycled aggregate concrete under the coupled compressive loading and sulfate erosion[J]. *J. Building Eng.* **99**, 111664 (2025).
11. Hewayde, E., Pachenari, A. & Al-Eleaj, H. Resistance of recycled aggregate concrete (RAC) subjected to Drying-Wetting cycles to attack of magnesium and sodium sulfates. *J. Eng.* **20200** (1), 9746341 (2020).

12. Li, Y. et al. Sulfate attack resistance of recycled aggregate concrete with NaOH-solution-treated crumb rubber. *Constr. Build. Mater.* **287**, 123044 (2021).
13. Santillan, L. R. et al. Long-term sulfate attack on recycled aggregate concrete immersed in sodium sulfate solution for 10 years. (2020).
14. Jia, P. et al. Performance evolution of recycled aggregate concrete under the coupled effect of freeze–thaw cycles and sulfate attack. *Appl. Sci.* **12** (14), 6950 (2022).
15. Bai, W. et al. Study on macroscopic mechanical properties and mesoscopic damage mechanism of recycled concrete with Metakaolin under sodium sulfate erosion environment. *J. Building Eng.* **70**, 106413 (2023).
16. Silva, Y. F. & Delvasto, S. Sulfate attack resistance of self-compacting concrete with residue of masonry. *Constr. Build. Mater.* **268**, 121095 (2021).
17. Jianwei, S. & Chen, Z. Influences of limestone powder on the resistance of concretes to the chloride ion penetration and sulfate attack. *Powder Technol.* **338**, 725–733 (2018).
18. Liang Guo, Y. et al. Improving sulfate attack resistance of concrete by using calcined Mg-Al-CO3 ldhs: adsorption behavior and mechanism. *Constr. Build. Mater.* **232**, 117256 (2020).
19. Xiao, Q. H. et al. Damage to recycled concrete with different aggregate substitution rates from the coupled action of freeze-thaw cycles and sulfate attack[J]. *Constr. Build. Mater.* **221**, 74–83 (2019).
20. Xiao, Q. H. et al. The deterioration law of recycled concrete under the combined effects of freeze-thaw and sulfate attack[J]. *Constr. Build. Mater.* **200**, 344–355 (2019).
21. Zhao, G., Li, J. & Shao, W. Effect of mixed chlorides on the degradation and sulfate diffusion of cast-in-situ concrete due to sulfate attack. *Constr. Build. Mater.* **181**, 49–58 (2018).
22. Devi, S. C. & Khan, R. A. Influence of graphene oxide on sulfate attack and carbonation of concrete containing recycled concrete aggregate. *Constr. Build. Mater.*, 250 (2020).
23. JGJ 52-. Quality and inspection method of sand and stone for ordinary concrete, Standardization Administration of the People's Republic of China, Beijing, China, 2006. (2006).

Acknowledgements
We express our sincere gratitude to the experts, teachers and students who have provided help for this article.

Author contributions
Y.F.: conceptualization, methodology, writing—original draft. Q.Z.: supervision, project administration, resources. Q.S: conceptualization, writing—review and editing. S.C.: methodology, writing—review and editing. H.S: conceptualization, writing—review and editing. F.Z.: writing—review and editing, supervision. C.B.: methodology, writing—review and editing. All authors have read and agreed to the published version of the manuscript.

Funding
No fund support.

Declarations

Competing interests
The authors declare no competing interests.

Additional information
Correspondence and requests for materials should be addressed to Y.F.

Reprints and permissions information is available at www.nature.com/reprints.

Publisher's note Springer Nature remains neutral with regard to jurisdictional claims in published maps and institutional affiliations.

Open Access This article is licensed under a Creative Commons Attribution-NonCommercial-NoDerivatives 4.0 International License, which permits any non-commercial use, sharing, distribution and reproduction in any medium or format, as long as you give appropriate credit to the original author(s) and the source, provide a link to the Creative Commons licence, and indicate if you modified the licensed material. You do not have permission under this licence to share adapted material derived from this article or parts of it. The images or other third party material in this article are included in the article's Creative Commons licence, unless indicated otherwise in a credit line to the material. If material is not included in the article's Creative Commons licence and your intended use is not permitted by statutory regulation or exceeds the permitted use, you will need to obtain permission directly from the copyright holder. To view a copy of this licence, visit http://creativecommons.org/licenses/by-nc-nd/4.0/.

© The Author(s) 2025